JOURNAL OF GUIDANCE, CONTROL, AND DYNAMICS
Vol. 18, No. 3, May–June 1995

Optimal Sliding-Mode Control of a Flexible Spacecraft Under Stochastic Disturbances

Alok Sinha*
Pennsylvania State University, University Park, Pennsylvania 16802
and
David W. Miller†
Massachusetts Institute of Technology, Cambridge, Massachusetts 02139

A new optimal sliding-mode (OSM) controller is developed for a linear stochastic system and applied to the Middeck Active Control Experiment (MACE), which represents the control structure interaction problem for a precision spacecraft. The OSM controller minimizes the expected value of a quadratic objective function consisting of only states with the constraints that esimated states always remain on the intersection of sliding hyperplanes. This controller is designed for two subsets of MACE problems: a single-input, single-output gimbal inertial pointing problem and a three-input, three-output torque wheel attitude control problem. Using numerical simulations, performance of the OSM controller is compared to that of the classical linear quadratic Gaussian controller. The OSM controllers are digitally implemented on the development model of MACE. The experimental results are shown to be in good agreement with theoretical results.

Nomenclature

A	= system matrix
B	= input matrix
C	= output matrix
$E(\cdot)$	= expected value
$F(S)$, $F_S(S)$, $F_G(S)$	= controller transfer functions
G	= $m \times n$ matrix defining sliding hyperplanes
H	= similarity transformation matrix
I_n	= n-dimensional identity matrix
J, J_g, J_s	= quadratic objective functions
K	= defined by Eq. (27)
K_F	= gain matrix for Kalman filter
K_G	= linear quadratic Gaussian controller gain matrix
L	= disturbance matrix
m	= number of inputs
n	= number of states
P	= defined by Eq. (7)
p	= number of outputs
Q	= symmetric positive-semidefinite matrix
$q(t)$	= transformed state vector, defined by Eq. (A1)
$q_1(t)$	= vector containing first $n - m$ elements of $q(t)$
$q_2(t)$	= vector containing last m elements of $q(t)$
S	= Laplace transformation variable
$\underline{S}(t)$	= defined by Eq. (11)
s_i	= variable defining ith sliding hyperplane
t	= time
$U(t)$	= control input vector
$V(t)$	= state estimation error vector
$X(t)$	= state vector
$X_e(t)$	= estimated state vector
$Y(t)$	= output vector
$\Gamma(S)$	= open-loop transfer function
$\Delta(S)$	= sensitivity function
η	= a positive number
μ	= measure of boundary-layer thickness
ν	= η/μ
$\Psi(S)$	= closed loop transfer function relating disturbance and output

Received Dec. 11, 1992; revision received Feb. 17, 1994; accepted for publication July 25, 1994. Copyright © 1994 by the American Institute of Aeronautics and Astronautics, Inc. All rights reserved.

*Associate Professor, Department of Mechanical Engineering. Member AIAA.

†Principal Research Scientist, Space Engineering Research Center. Member AIAA.

I. Introduction

THE active control of a flexible spacecraft is an important area of research. The future generation of spacecraft will consist of a highly flexible structure with multiple payloads.[1] The requirements on pointing accuracies for the attached payloads are going to be much higher. Hence, it is inevitable that the control bandwidth required for precision pointing will excite the flexible structural modes. This is known as control structure interaction (CSI). In addition, the controller for each payload must reject the disturbances caused by simultaneous maneuvering of other payloads. To develop design guidelines for a precision spacecraft with multiple payloads, the Middeck Active Control Experiment (MACE) is being developed by the Space Engineering Research Center at the Massachusetts Institute of Technology (MIT).[2] The development model (DM) shown in Fig. 1 is the first of three sets of hardware to be developed under the MACE program.[3] The DM is composed of a flexible bus that supports a two-axis gimbaling payload and a dummy mass that will be replaced by a second gimbal in the near future. A three-axis torque wheel assembly is placed for the attitude control of the flexible bus. The various identification and control experiments are scheduled to be performed in the middeck of the Space Shuttle in 1994. The control problem is set as a stochastic regulator problem where stochastic broadband torque disturbances have to be rejected in order to obtain a required pointing accuracy of a payload.[4]

This paper deals with the development of a new optimal sliding-mode (OSM) control system for a linear stochastic system and its application to the DM of MACE. Since all the states cannot be known for a flexible structure, the control law must be based on the measured outputs. The states are estimated using the well-known Kalman filter.[5] Then, m number of sliding hyperplanes are defined in the estimated state space, where m is the number of inputs. The control law is defined such that estimated states always remain on the intersection of the chosen set of hyperplanes (Fig. 2). These hyperplanes are chosen to minimize a quadratic objective function J consisting of only states. This optimization task reduces to the solution of a standard linear quadratic problem in $n - m$ dimensions where n is the number of states. In other words, $n - m$ closed-

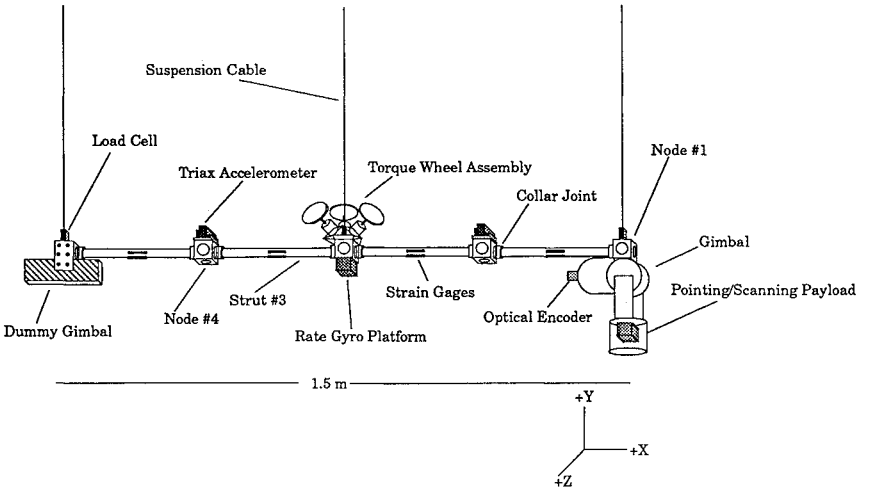

Fig. 1 Development model of MACE.

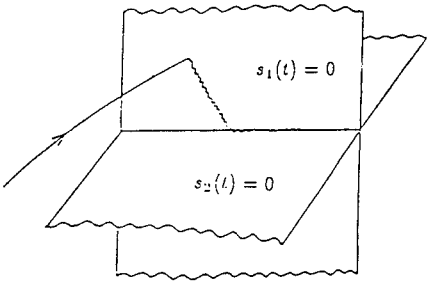

Fig. 2 Sliding manifold.

loop poles are determined by the optimal choice of sliding hyperplanes. The remaining m closed-loop poles are governed by the thicknesses of boundary layers around hyperplanes. For a stochastic linear system, it is shown that the aforementioned control law minimizes the expected value of the quadratic objective function J. Here, the constraints for optimization are that all the estimated states are always on the intersection of sliding hyperplanes. Compared to the well-known linear quadratic Gaussian (LQG) control[5] in which the objective function must contain the input term, the OSM control law can be viewed as an alternate way of optimizing the system.

The sliding-mode control technique was originally developed in the former Soviet Union[6,7] and has recently attracted attention of researchers in other countries.[8,9] Sinha and Kao[10,11] have studied the asymptotic behavior of closed-loop systems inside boundary layers for a full-state feedback deterministic control of vibration in flexible structures. Kao and Sinha[12] examined the robustness of the sliding-mode control system with estimated states to spillover phenomena caused by residual modes of vibration. However, they did not consider a stochastic system. Yurkovich et al.[13] have developed a model reference sliding-mode control law for a deterministic flexible structure. They did not deal with the issue of optimality, and their controller does not guarantee the behavior of structures at those locations where sensors are not mounted.

First, the theoretical development of the OSM controller is presented for a linear stochastic system. Then, two subsets of MACE control problems are considered. The first control problem[3] deals with a single-input, single-output (SISO) system that pertains to controlling the inertial angle of the gimbal mounted payload subject to stochastic torque disturbance in the gimbal. The second problem deals with the attitude control of the flexible bus by torque wheels under stochastic disturbances. In each case, the sensitivity of the OSM controller is compared to that of the LQG controller for the similar level of performance in terms of disturbance rejection. Lastly, experimental results are obtained by digitally implementing OSM controllers and are compared with theoretical results.

II. Development of Sliding-Mode Control System

Consider the linear stochastic system

$$\frac{dX(t)}{dt} = AX(t) + BU(t) + L\xi(t) \tag{1}$$

$$Y(t) = CX(t) + \theta(t) \tag{2}$$

where states $X(t) \in R^n$, input $U(t) \in R^m$, and output $Y(t) \in R^p$. It is assumed that (A, B) and (A, C) are controllable and observable, respectively. The plant disturbance vector $\xi(t)$ and the sensor noise vector $\theta(t)$ contain independent white-noise processes with zero mean as their elements. Let their covariance matrices be defined as

$$E[\xi(t)\xi^T(\tau)] = Q_0\delta(t-\tau) \tag{3}$$

$$E[\theta(t)\theta^T(\tau)] = R_0\delta(t-\tau) \tag{4}$$

where $\delta(t-\tau)$ is the Dirac delta function.

Using the Kalman filter, the estimated state vector $X_e(t)$ is given by the relationship

$$\frac{dX_e(t)}{dt} = AX_e(t) + BU(t) + K_F[Y(t) - CX_e(t)] \tag{5}$$

where the gain matrix K_F is given by

$$K_F = PC^TR_0^{-1} \tag{6}$$

$$PA^T + AP + Q_0 - PC^TR_0^{-1}CP = 0 \tag{7}$$

For m inputs, m hyperplanes passing through the origin of the estimated state space are defined[12] as

$$s_i = g_i^T X_e(t), \qquad i = 1, 2, \ldots, m \tag{8}$$

If the estimated states never leave sliding hyperplanes, $ds_i/dt = 0$. This condition and Eq. (5) yield the following relationship for the equivalent controller:

$$U_{eq}(t) = -(GB)^{-1}[G(A - K_FC)X_e(t) + GK_FY(t)] \tag{9}$$

where

$$G = [g_1, g_2, \ldots, g_m]^T \tag{10}$$

From Eqs. (8) and (10),

$$\underline{S}(t) = GX_e(t) \tag{11}$$

where

$$\underline{S}(t) = [s_1(t), s_2(t), \ldots, s_m(t)]^T \tag{12}$$

The conditions for any initial state to reach the sliding manifold (intersection of sliding hyperplanes; Fig. 2) are called the reaching conditions, which are described as $s_i(ds_i/dt) < 0, i = 1, 2, \ldots, m$. To satisfy these reaching conditions, the control law is chosen as

$$U(t) = U_{eq}(t) - (GB)^{-1}\text{diag}(\eta)\text{sgn}[\underline{S}(t)] \tag{13}$$

where $\text{diag}(\eta)$ is a diagonal matrix with the ith diagonal equal to a positive number η_i. The ith element of the vector $\text{sgn}[\underline{S}(t)]$ is defined as

$$\text{sgn}[s_i(t)] = \begin{cases} +1 & \text{if} \quad s_i(t) > 0 \\ -1 & \text{if} \quad s_i(t) < 0 \end{cases} \tag{14}$$

To eliminate the chattering behavior caused by the sgn function, a boundary layer[8] is introduced around each sliding hyperplane by replacing the sgn function in Eq. (13) by the saturation function. Hence, the control law (13) is modified to be

$$U(t) = U_{eq}(t) - (GB)^{-1}\text{diag}(\eta)\text{sat}[\underline{S}(t)] \tag{15}$$

The ith element of $\text{sat}[\underline{S}(t)]$ is described as

$$\text{sat}[s_i(t)] = \begin{cases} \text{sgn}[s_i(t)] & \text{if } |s_i(t)| > \mu_i \\ s_i(t)/\mu_i & \text{otherwise} \end{cases} \tag{16}$$

where μ_i is a measure of the boundary-layer thickness around the ith hyperplane. Although $\text{sat}[\underline{S}(t)]$ is a nonlinear function, the closed-loop system is linear inside boundary layers where it can be shown that

$$\frac{ds_i}{dt} = -\frac{\eta_i}{\mu_i}s_i(t) \tag{17}$$

For state estimation, $X_e(0)$ is typically set to zero. In this case, $\underline{S}(0) = 0$ and the solution of Eq. (17) indicates that $\underline{S}(t) = 0$. Therefore, estimated states will never leave hyperplanes and the resulting feedback control law will be linear. Using Eqs. (9), (15), and (16), the effective linear control law is given by

$$U(t) = -(GB)^{-1}\left[G\left(A - K_FC + \frac{\eta}{\mu}I_n\right)X_e(t) + GK_FY(t)\right] \tag{18}$$

Without any loss of generality, η_i and μ_i have been assumed to be η and μ, respectively. Note that the control law utilizes the direct feedback of the output in addition to the feedback of estimated states.

III. Dynamics of Closed-Loop System

Using Eqs. (1), (5), and (18), the dynamics of the closed-loop system can be described as

$$\begin{bmatrix} \dfrac{dX(t)}{dt} \\ \dfrac{dV(t)}{dt} \end{bmatrix} = \begin{bmatrix} A - \Omega(A + \nu I_n) & \Omega(A + \nu I_n) - \Omega K_FC \\ 0 & A - K_FC \end{bmatrix} \times \begin{bmatrix} X(t) \\ V(t) \end{bmatrix} + \begin{bmatrix} L & -\Omega K_F \\ L & -K_F \end{bmatrix}\begin{bmatrix} \xi(t) \\ \theta(t) \end{bmatrix} \tag{19}$$

where

$$V(t) = X(t) - X_e(t) \tag{20}$$

$$\nu = \eta/\mu \tag{21}$$

$$\Omega = B(GB)^{-1}G \tag{22}$$

Equation (19) indicates that the eigenvalues of the closed-loop system are those of $A - \Omega(A + \nu I_n)$ and $A - K_FC$. The dynamics of the state estimation error $V(t)$ is governed by the eigenvalues of $A - K_FC$. It is also clear that $A - \Omega(A + \nu I_n)$ is the closed-loop system matrix for the full-state regulator problem. Hence, the eigenvalue separation property holds.[5]

Lemma 1. The m eigenvalues of $A - \Omega(A + \nu I_n)$ are $-\nu$ and the remaining $n - m$ eigenvalues can be arbitrarily placed in the S plane by a proper choice of G since the system (A, B) is controllable.

Proof. The proof directly follows from the paper by Utkin and Yang.[14] For the sake of completeness, this proof is given in the Appendix.

IV. Optimal Choice of Sliding Hyperplanes or Matrix G

For the full-state and deterministic regulator problem, the matrix G will be sought to minimize the following quadratic objective function:

$$J = \int_0^\infty X^T(t)QX(t)\,dt \tag{23}$$

where Q is symmetric and positive semidefinite. From Eqs. (A1) and (23),

$$J = \int_0^\infty qT(t)(H^{-1})^T QH^{-1}q(t)\,dt \tag{24}$$

Since the signs of eigenvalues are preserved under congruence transformation,[15] the matrix $(H^{-1})^T QH^{-1}$ is symmetric and positive semidefinite. Define

$$(H^{-1})^T QH^{-1} = \begin{bmatrix} Q^1 & N \\ N^T & R \end{bmatrix} \tag{25}$$

Now, Eq. (24) can be written as

$$J = \int_0^\infty q_1^T(t)Q_1q_1(t) + 2q_1^T(t)Nq_2(t) + q_2^T(t)Rq_2(t)\,dt \tag{26}$$

Equations (26) and (A7) represent a standard linear quadratic problem[14] provided $R > 0$. If Q is chosen to be positive definite, R is guaranteed to be positive definite because the signs of eigenvalues are preserved under congruence transformation. When Q is not positive definite, e.g., $Q = C^TC$ with $p < n$, R may not be positive definite. If R does not turn out to be positive definite, as it will be seen in Sec. V, it has to be arbitrarily chosen to be a positive-definite function. In this case, a new Q will be defined according to Eq. (25).

The gain matrix K that minimizes Eq. (26) is[5]

$$K = R^{-1}\left[A_{12}^TP_2 + N^T\right] \tag{27}$$

where

$$P_2\left(A_{11} - A_{12}R^{-1}N^T\right) + \left(A_{11}^T - NR^{-1}A_{12}^T\right)P_2 - P_2A_{12}R^{-1}A_{12}^TP_2 + Q_1 - NR^{-1}N^T = 0 \tag{28}$$

The optimal G is then obtained by substituting Eq. (27) into Eq. (A10).

Lemma 2. For the stochastic system (1), (2), and (5), the G chosen on the basis of Eq. (27) minimizes the function

$$J_s = E\left[\lim_{T\to\infty}\frac{1}{T}\int_0^T X(t)^TQX(t)\,dt\right] \tag{29}$$

It should be noted that the constraint for minimization of the function (29) is $\underline{S}(t) = GX_e(t) = 0$.

Proof. For the Kalman filter, it is well known[5] that

$$E[X_e(t)V^T(t)] = 0 \tag{30}$$

Using Eq. (30), it can be shown that

$$E[X(t)^TQX(t)] = E[X_e(t)^TQX_e(t)] + \text{tr}(Q\Sigma) \tag{31}$$

where

$$\Sigma = E[V(t)V(t)^T] \tag{32}$$

From Eq. (19), $\text{tr}(Q\Sigma)$ is independent of the input $U(t)$. Hence, the minimization problem described in Lemma 2 can be recast as follows: Find G that minimizes

$$J_m = E\left[\lim_{T\to\infty}\frac{1}{T}\int_0^T X_e(t)^TQX_e(t)\,dt\right] \tag{33}$$

subject to Eq. (5) and $\underline{S}(t) = GX_e(t) = 0$.

Equation (5) can be rewritten as

$$\frac{dX_e}{dt} = AX_e(t) + BU(t) + K_F\chi(t) \tag{34}$$

where

$$\chi(t) = Y(t) - CX_e(t) \tag{35}$$

It is recalled that the function $\chi(t)$ is known as the innovation process. It is well known[16] that this is a white-noise process with intensity R_0. Using the similarity transformation matrix $q_e(t) = HX_e(t)$, an equation similar to Eq. (A7) is obtained:

$$\frac{dq_{e1}}{dt} = A_{11}q_{e1}(t) + A_{12}q_{e2}(t) + (HK_F)_{nm}\chi(t) \tag{36}$$

where $q_e(t) = [q_{e1}^T(t)\, q_{e2}^T(t)]^T$ and the matrix $(HK_F)_{nm}$ is the first $n - m$ row of the matrix HK_F. The corresponding form of the objective function (33) under the similarity transformation will be

$$J_m = E\left[\lim_{T\to\infty}\frac{1}{T}\int_0^T q_{e1}^T Q_1 q_{e1} + 2q_{e1}^T N q_{e2} + q_{e2}^T R q_{e2}\, dt\right] \tag{37}$$

It should be recalled that $\underline{S}(t) = q_{e2}(t) + Kq_{e1}(t)$. Using the stochastic regulator theory[16] with full-state feedback, it is obvious that the matrix G (or K) that minimizes Eq. (26) also minimizes Eq. (37), which is the same as Eq. (33). This completes the proof.

V. Application to MACE

The OSM control law is developed and digitally implemented for two subsets of the MACE control problem. The first problem deals with SISO payload inertial pointing and the second problem pertains to three-input, three-output attitude control. Using numerical simulations,[17] performance of the OSM controller is compared to that of an LQG controller for which the following objective function is minimized:

$$J_g = \lim_{T\to\infty} E\left[\frac{1}{T}\int_0^T Y(t)^T Y(t) + \rho U(t)^T U(t)\, dt\right] \tag{38}$$

The LQG controller transfer function is described as

$$U(S) = -F_G(S)Y(S) \tag{39}$$

where

$$F_G(S) = K_G(SI_n - A + BK_G + K_F C)^{-1}K_F \tag{40}$$

and K_G is the LQG controller gain matrix.

Using Eqs. (5) and (18), the OSM controller transfer function is obtained as

$$U(S) = -F_S(S)Y(S) \tag{41}$$

where

$$F_S(S) = K_S(SI_n - A + BK_S + K_F C)^{-1} \times [K_F - B(GB)^{-1}GK_F] + (GB)^{-1}GK_F \tag{42}$$

and

$$K_S = (GB)^{-1}G(A + \nu I_n - K_F C) \tag{43}$$

As mentioned in Sec. I, the objective of the controller design is to reject stochastic broadband torque disturbances. Hence, the performance of the control system is measured by the magnitude of the closed-loop transfer function relating the disturbance and the output vectors. This transfer function is defined as

$$\Psi(S) = [I_p + \Gamma(S)F(S)]^{-1}\Gamma(S) \tag{44}$$

where $\Gamma(S) = C(SI_n - A)^{-1}B + D$ is the open-loop transfer function and $F(S)$ is the controller transfer function as defined by $F_S(S)$ and $F_G(S)$ for OSM and LQG controllers, respectively.

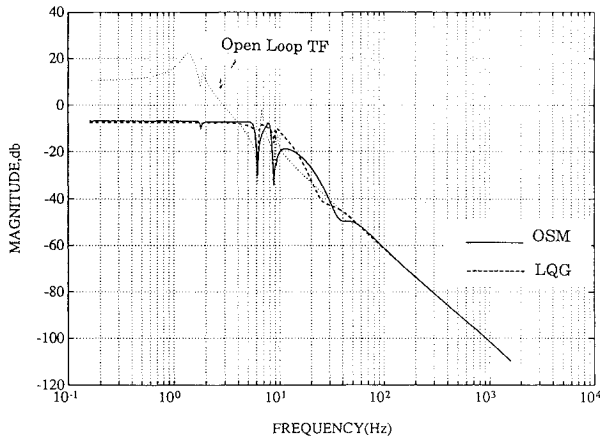

Fig. 3 SISO closed-loop transfer functions ($R = 4$, $\rho = 0.01$).

For the sake of discussion in Secs. V.A and V.B, the well-known sensitivity function[5] is defined as

$$\Delta(S) = [I_p + \Gamma(S)F(S)]^{-1} \tag{45}$$

Anderson and Moore[5] have shown that a smaller $\Delta(S)$ implies a greater robustness to structured parametric uncertainties. For a SISO system, the function $\Delta(S)$ is the ratio of a percentage change in the closed-loop transfer function and the percentage change in the open-loop transfer function.

The state-space model of $F_S(S)$ is discretized using the tustin method for the digital implementation of OSM controller with AC100.[18] The sampling frequency is taken to be 500 Hz. The experimental results are compared with theoretical results.

A. Single-Input, Single-Output System

The objective is to inertially point the payload about the z axis while a band-limited white-noise disturbance torque is introduced through the z-axis gimbal motor, which also provides the control input (torque). The response of the flexible bus in the x-y plane is included in the system model. The inertial angle of the payload is measured by the stabilized integral of a rate gyro signal. The stabilized integrator acts as a first-order high-pass filter at frequencies below 0.03 Hz and integrates the signal above 0.03 Hz.

Model

The dynamics of this SISO plant is obtained by experimentally measuring[3] the transfer function representing the ratio of stabilized integration of rate gyro signal and the volatge into the gimbal torque motor amplifier. This transfer function represents the dynamics of motor amplifier, the gimbal/flexible bus, the rate gyro on the payload, the eight-pole 150-Hz Bessel antialiasing filter, the 0.03-Hz stabilized integrator, and the 500-Hz digital delay. The SISO transfer function was then curve fitted[3] using five complex poles, four complex zeros, a static gain, and a time delay. This time delay represents all the delays associated with the processing delay, the antialiasing filters, and rate gyro dynamics. A third-order Padé approximation[17] is used to represent the effects of time delay. The state-space model representing the measured transfer function is then developed for the controller design. The dimension of this state-space model is 13.

Controller Design

For the OSM control, $Q = C^T C$ is chosen first. For this Q, R defined in Eq. (26) turns out be zero. Hence, R is arbitrarily taken to be a positive number, and it plays the same role as ρ does for the LQG control [Eq. (38)]. The inverse of R can be described as a measure of the control authority.

First, R is chosen to be 4. The closed-loop transfer function $\Psi(S)$ relating the disturbance and the output is shown in Fig. 3. This is overlayed with the open-loop transfer function calculated using the fitted model. Then, the LQG controller is designed with the same Kalman filter and $\rho = 0.01$ such that $E(YY^T)$ is almost

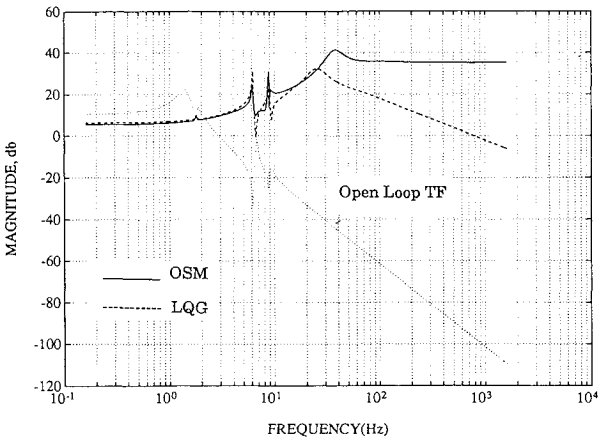

Fig. 4 OSM and LQG controller transfer functions.

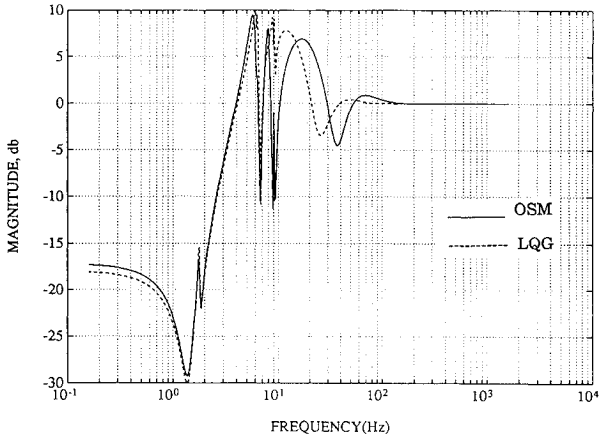

Fig. 5 Magnitudes of sensitivity functions ($R = 4$, $\rho = 0.01$).

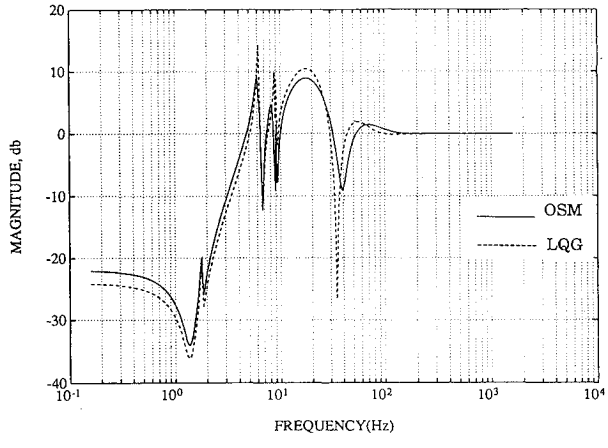

Fig. 6 Magnitudes of sensitivity functions ($R = 0.6$, $\rho = 10^{-4}$).

the same as that for the OSM controller. The frequency response of the LQG closed-loop transfer function $\Psi(S)$ is also shown in Fig. 3. Both controllers lead to similar levels of performance in terms of disturbance rejection. In Fig. 4, LQG and OSM controller transfer functions are plotted. Focusing attention around 6–9 Hz, it is seen that the LQG controller results in plant inversion whereas the OSM controller does so to a lesser degree. The magnitudes of the sensitivity functions $\Delta(S)$ for both controllers are presented in Fig. 5. It can be concluded that the sensitivity of the LQG controller is greater than that of the OSM controller.

Next, results are examined for $R = 0.6$ and $\rho = 1 \times 10^{-4}$, which leads to almost equal values of $E(YY^T)$ for both the controllers. Again, it is concluded that the OSM controller is less sensitive than the LQG controller for the similar level of performance (Fig. 6).

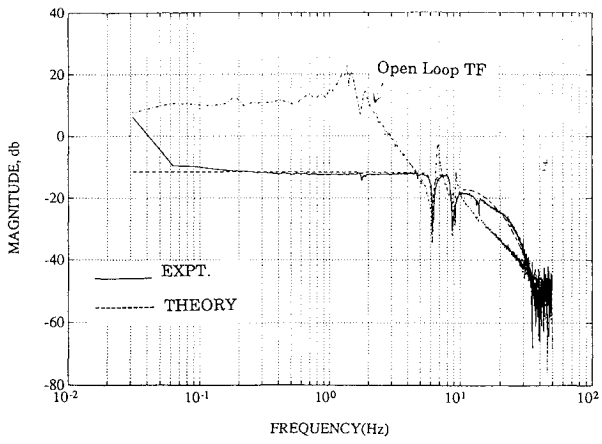

Fig. 7 Experimental OSM closed-loop transfer function ($R = 0.6$).

Experimental Results

The OSM controllers for $R = 4$ and 0.6 have been digitally implemented. The experimental closed-loop transfer function compares well with the theoretical closed-loop transfer function (Fig. 7). The reduction in the root-mean-square (rms) value of the inertial gimbal position is about 20 dB. It should be noted that good performance is obtained with the controller derived on the basis of a model developed several months ago. LQG controllers that stabilized the plant when this model was new have subsequently been destabilizing due to shifts in dynamics caused by reassembly of the hardware. In this sense,[3] the OSM controller seems to be more robust than the LQG controller.

B. Three-Input, Three-Output System

The three inputs are independent torques produced by three torque wheels whereas the three outputs are the inertial angles of the flexible bus, which are obtained by the stabilized integration of the rate gyro signals. The broadband torque disturbances are also provided by torque wheels, i.e., $L = B$. The objective is to control the attitudes of the flexible bus under the torque disturbances.

Model

The dynamic model is obtained by measuring three single-input, three-output (SITO) transfer functions by applying only one input at a time. On the basis of these three SITO transfer functions, a multi-input, multi-output (MIMO) model is obtained. A total time delay of 15.2 ms was estimated to be present in each input channel. Each of these time delays is modeled by a fourth-order Padé approximation. Excluding time delays, the order of the state-space model is 52. Neglecting the higher modes, this model is reduced to have 36 states. This reduced-order model is then augmented to include the state-space model representing the Padé approximations for time delays. Hence, the controller is designed on the basis of a model with 48 states.

Controller Design

For the OSM controller design, Q is again chosen to be C^TC. The corresponding R in Eq. (26) turns out to be nearly singular. Therefore, R is chosen to be $\rho_s I_3$, where ρ_s is a positive number.

In Figs. 8–10, the magnitudes of the diagonal elements of the closed-loop transfer function matrix $\Psi(S)$ are shown for the OSM controller with $\rho_s = 0.03$. The maximum singular value of the corresponding sensitivity function $\Delta(S)$ is shown in Fig. 11. In Fig. 11, the maximum singular value of the sensitivity function $\Delta(S)$ is also plotted for a LQG controller with $\rho = 0.01$. This value of ρ is chosen so that the LQG controller led to almost the same values of $E(YY^T)$ as those for the OSM controller. Comparing maximum singular values in Fig. 11, it can be said that the LQG controller is more sensitive to plant parameter variations than the OSM controller.

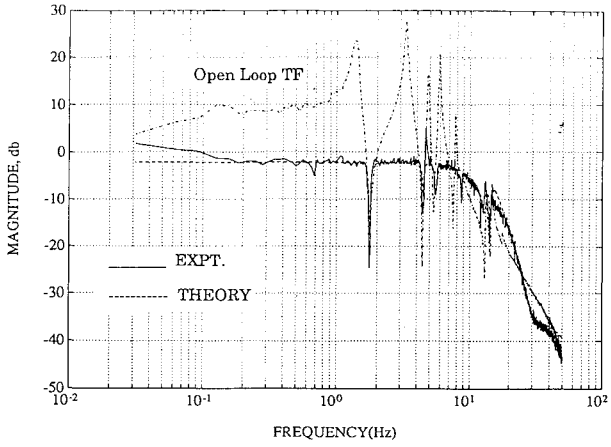

Fig. 8 *X*-axis three-input, three-output (TITO) closed-loop transfer function with OSM controller.

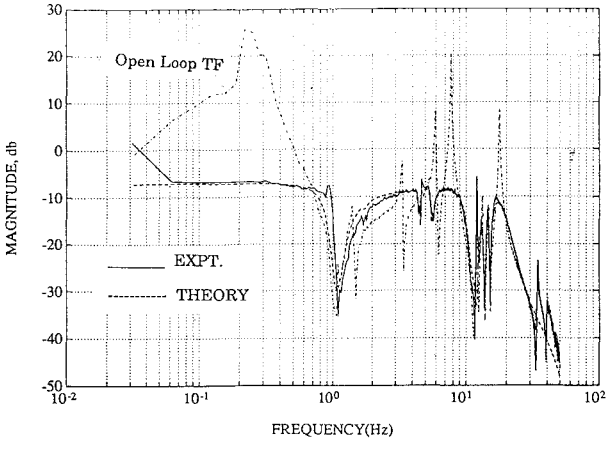

Fig. 9 *Y*-axis TITO closed-loop transfer function with OSM controller.

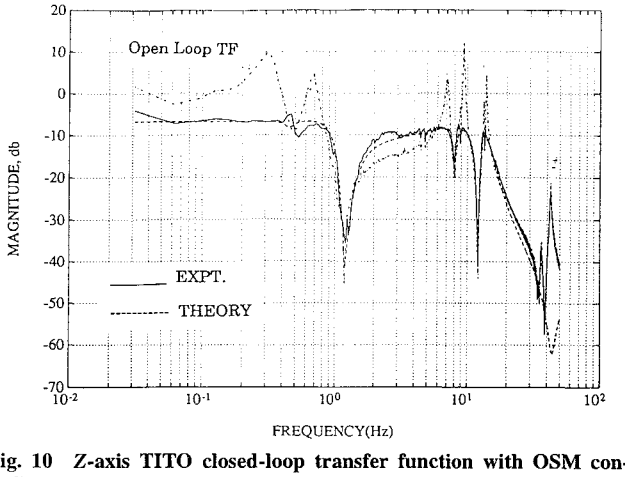

Fig. 10 *Z*-axis TITO closed-loop transfer function with OSM controller.

Experimental Results

The OSM controller is digitally implemented and the stochastic disturbance torque is introduced about only one axis at a time. The experimental results for the OSM controller with $\rho_s = 0.03$ are shown in Figs. 8–10. It is clear that experimental results compare well with theoretical results. The reductions in the rms values of the angular positions are about 16.5 dB in the x direction, about 17.25 dB in the y direction, and about 8.35 dB in the z direction. Although the LQG controller derived with $\rho = 0.01$ leads to similar levels of performance in theory, it led to an unstable closed-loop system when implemented.

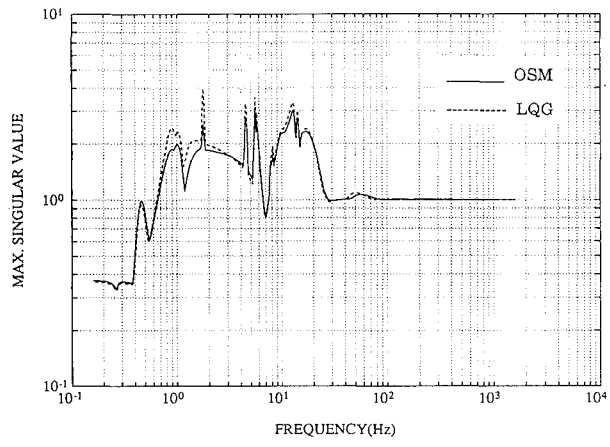

Fig. 11 Maximum singular values of sensitivity functions for TITO system.

VI. Summary and Conclusions

A new optimal OSM controller has been developed for a linear stochastic system. The states are estimated using the Kalman filter and m number of sliding hyperplanes are defined in the estimated state space, where m is the number of inputs. It has been shown that m controller poles are determined by the thicknesses of boundary layers and remaining $n - m$ poles are governed by the choice of sliding hyperplanes, where n is the number of states. The sliding hyperplanes are chosen to minimize the expected value of a quadratic objective function consisting of only states. This task requires the solution of a linear quadratic problem in $n - m$ dimensions.

The OSM controller has been applied to the developmental model of the MACE. Two subsets of control problems have been considered: a SISO payload inertial pointing problem and a three-input, three-output attitude control problem. The results from numerical simulations indicate that the sensitivity function for the OSM controller is smaller than that for the LQG controller.

For both subsets of control problems, experimental closed-loop transfer functions relating the disturbance and the output compare well with theoretical results. The experimental results indicate that the OSM controller can result in significant reductions in the rms values of the outputs.

Appendix: Proof of Lemma 1

Let the columns of a matrix P_1 be composed of basis vectors of the null space[14,15] of B^T. Define a similarity transformation

$$q(t) = HX(t) \tag{A1}$$

where

$$H = [P_1 \quad B]^T \tag{A2}$$

From Eqs. (1) and (A1) and ignoring the disturbance,

$$\frac{dq(t)}{dt} = \boldsymbol{A}q(t) + \boldsymbol{B}U(t) \tag{A3}$$

where

$$\boldsymbol{A} = HAH^{-1} \tag{A4}$$

$$\boldsymbol{B} = HB \tag{A5}$$

Because of the special structure of H, it can be seen that the first $n-m$ rows of $\boldsymbol{B}$ will be zero. Hence, decomposing $q(t)$ as $[q_1(t)^T \; q_2(t)^T]^T$, where $q_1(t)$ and $q_2(t)$ are $(n - m)$ and m-dimensional vectors, Eq. (A3) can be written as

$$\begin{bmatrix} \dfrac{dq_1}{dt} \\ \dfrac{dq_2}{dt} \end{bmatrix} = \begin{bmatrix} A_{11} & A_{12} \\ A_{21} & A_{22} \end{bmatrix} \begin{bmatrix} q_1(t) \\ q_2(t) \end{bmatrix} + \begin{bmatrix} 0 \\ B_r \end{bmatrix} U(t) \tag{A6}$$

or

$$\frac{dq_1}{dt} = A_{11}q_1(t) + A_{12}q_2(t) \tag{A7}$$

$$\frac{dq_2}{dt} = A_{21}q_1(t) + A_{22}q_2(t) + BrU(t) \tag{A8}$$

Now, $\underline{S}(t)$ can be expressed as

$$\underline{S}(t) = q_2(t) + Kq_1(t) \tag{A9}$$

For a full-state regulator problem, Eq. (11) will take the form of $\underline{S}(t) = GX(t)$. Hence, from Eqs. (A1) and (A9),

$$G = [K \quad I_m]H \tag{A10}$$

Substituting Eq. (A9) into Eq. (A7) and using Eq. (17), system dynamics for the full-state regulator problem can be represented as

$$\begin{bmatrix} \frac{dq_1}{dt} \\ \frac{d\underline{S}}{dt} \end{bmatrix} = \begin{bmatrix} A_{11} - A_{12}K & A_{12} \\ 0 & -\nu I_m \end{bmatrix} \begin{bmatrix} q_1(t) \\ \underline{S}(t) \end{bmatrix} \tag{A11}$$

Using Eqs. (A1) and (A9), it is recognized that $X(t)$ and $[q_1^T \underline{S}(t)^T]^T$ are related by similarity transformation. Since the closed-loop system matrix for the full-state regulator problem is $A - \Omega(A + \nu I_n)$ and the eigenvalues remain unchanged under similarity transformation, the eigenvalues of $A - \Omega(A + \nu I_n)$ are those of $A_{11} - A_{12}K$ and $-\nu I_m$. Hence, m eigenvalues of $A - \Omega(A + \nu I_n)$ are $-\nu$ and the remaining $n - m$ eigenvalues are those of $A_{11} - A_{12}K$.

When $\underline{S}(t) = 0, q_2(t) = -Kq_1(t)$. In view of Eq. (A7), K is a state feedback vector. Utkin and Yang[14] have shown that (A_{11}, A_{12}) is controllable if (A, B) is controllable. Hence, eigenvalues of $A_{11} - A_{12}K$ can be arbitrarily placed in the S plane by a proper choice of K. Since the choice of K directly yields G [Eq. (A10)], it is clear that $n - m$ eigenvalues of $A - \Omega(A + \nu I_n)$ can be arbitrarily placed by a proper choice of G. This completes the proof.

Acknowledgments

This work was performed while the first author was on sabbatical at the MIT Space Engineering Research Center. The first author wishes to thank Professor E. F. Crawley for his help. The authors also thank E. Saarmaa for helping with the experiments.

References

[1]Laskin, R. A., and Sirlin, S. W., "Future Payload Isolation and Pointing System Technology," *Journal of Guidance, Control, and Dynamics*, Vol. 9, No. 4, 1986, pp. 469–477.

[2]Miller, D. W., de Luis, J., and Crawley, E. F., "Dynamics and Control of Multipayload Platforms: The Middeck Active Control Experiment (MACE)," International Astronautical Federation, Paper IAF-90-292, Dresden, Germany, Oct. 1990.

[3]Miller, D. W., Saarmaa, E., and Jacques, R. N., "Preliminary Structural Control Results from the Middeck Active Control Experiments (MACE)," AIAA Paper 92-2138, 1992.

[4]Mercadel, M., "The Middeck Active Control Experiment First Sample Problem: Sensor and Actuator Selection, Sensor and Actuator Pairing," Massachusetts Institute of Technology, SERC Rept. 6-91-R, Cambridge, MA, June 1991.

[5]Anderson, B. D. O., and Moore, J. B., *Optimal Control: Linear Quadratic Methods*, Prentice-Hall, Englewood Cliffs, NJ, 1990.

[6]Utkin, V. I., "Variable Structure Systems with Sliding Modes: A Survey," *IEEE Transactions on Automatic Control*, Vol. AC-22, No. 2, 1977, pp. 212–222.

[7]Utkin, V. I., "Variable Structure Systems: Present and Future," *Automation and Remote Control*, Vol. 44, No. 9, 1983, pp. 1105–1119.

[8]Slotine, J. J. E., "The Robust Control of Robot Manipulators," *International Journal of Robotic Research*, Vol. 4, No. 2, 1985, pp. 49–64.

[9]Oz, H., and Mostafa, O., "Variable Structure Control System (VSCS) Maneuevering of a Flexible Spacecraft," *Journal of the Astronautical Sciences*, Vol. 36, No. 3, 1988, pp. 311–344.

[10]Sinha, A., and Kao, C. K., "Independent Modal Sliding Mode Control of Vibration in Flexible Structures," *Journal of Sound and Vibration*, Vol. 147, No. 2, 1991, pp. 352–358.

[11]Kao, C. K., and Sinha, A., "Coupled Modal Sliding Mode Control of Vibration in Flexible Structures," *Journal of Guidance, Control, and Dynamics*, Vol. 15, No. 1, 1992, pp. 65–73.

[12]Kao, C. K., and Sinha, A., "Sliding Mode Control of Vibration in Flexible Structures Using Estimated States," *Proceedings of the American Control Conference*, Vol. 3, 1990, pp. 2467–2474.

[13]Yurkovich, S., Ozgunner, U., and Al-Abbas, F., "Model Reference Sliding Mode Adaptive Control for Flexible Structures," *Journal of Astronautical Sciences*, Vol. 36, No. 3, 1988, pp. 285–310.

[14]Utkin, V. I., and Yang, K. D., "Methods for Constructing Discontinuity Planes in Multidimensional Variable Structure Systems," *Automation and Remote Control*, Vol. 39, No. 10, 1978, pp. 1466–1470.

[15]Strang, G., *Linear Algebra and Its Applications*, Harocourt Brace Javanovich, San Diego, 1988.

[16]Kwakernaak, H., and Sivan, R., *Linear Optimal Control Systems*, Wiley, New York, 1972.

[17]*PRO-MATLAB User's Guide*, The Mathworks, Natick, MA, 1990.

[18]*Using the AC-100: AC-100 User's Guide v2.4.03A*, Integrated Systems, Santa Clara, CA, Nov. 1990.